AIChE

A Superstructure-Based Optimal Synthesis of PSA Cycles for Post-Combustion CO_2 Capture

Anshul Agarwal and Lorenz T. Biegler
Collaboratory for Process and Dynamic Systems Research, National Energy Technology Laboratory, Morgantown, WV 26507
Chemical Engineering Dept., Carnegie Mellon University, Pittsburgh, PA 15213

Stephen E. Zitney
Collaboratory for Process and Dynamic Systems Research, National Energy Technology Laboratory, Morgantown, WV 26507

DOI 10.1002/aic.12107
Published online November 9, 2009 in Wiley InterScience (www.interscience.wiley.com).

Recent developments have shown pressure/vacuum swing adsorption (PSA/VSA) to be a promising option to effectively capture CO_2 from flue gas streams. In most commercial PSA cycles, the weakly adsorbed component in the mixture is the desired product, and enriching the strongly adsorbed CO_2 is not a concern. On the other hand, it is necessary to concentrate CO_2 to high purity to reduce CO_2 sequestration costs and minimize safety and environmental risks. Thus, it is necessary to develop PSA processes specifically targeted to obtain pure strongly adsorbed component. A multitude of PSA/VSA cycles have been developed in the literature for CO_2 capture from feedstocks low in CO_2 concentration. However, no systematic methodology has been suggested to develop, evaluate, and optimize PSA cycles for high purity CO_2 capture. This study presents a systematic optimization-based formulation to synthesize novel PSA cycles for a given application. In particular, a novel PSA superstructure is presented to design optimal PSA cycle configurations and evaluate CO_2 capture strategies. The superstructure is rich enough to predict a number of different PSA operating steps. The bed connections in the superstructure are governed by time-dependent control variables, which can be varied to realize most PSA operating steps. An optimal sequence of operating steps is achieved through the formulation of an optimal control problem with the partial differential and algebraic equations of the PSA system and the cyclic steady state condition. Large-scale optimization capabilities have enabled us to adopt a complete discretization methodology to solve the optimal control problem as a large-scale nonlinear program, using the nonlinear optimization solver IPOPT. The superstructure approach is demonstrated for case studies related to post-combustion CO_2 capture. In particular, optimal PSA cycles were synthesized, which maximize CO_2 recovery for a given purity, and minimize overall power consumption. The results show the potential of the superstructure to predict PSA cycles with up to 98% purity and recovery of CO_2. Moreover, for recovery of around 85% and purity of over 90%, these cycles can recover CO_2 from atmospheric flue gas with a low power consumption of

Correspondence concerning this article should be addressed to L. T. Biegler at lb01@andrew.cmu.edu.

465 kWh tonne^{-1} CO_2. The approach presented is, therefore, very promising and quite useful for evaluating the suitability of different adsorbents, feedstocks, and operating strategies for PSA, and assessing its usefulness for CO_2 capture. Published 2009 American Institute of Chemical Engineers *AIChE J*, 56: 1813–1828, 2010
Keywords: adsorption/gas, optimization, design

Introduction

Today, fossil fuels provide about 85% of the global energy demand and the outlook is that they will remain the dominant source of energy for decades to come. Consequently, global energy-related CO_2 emissions, especially from power plants that burn fossil fuels, have increased, thereby increasing CO_2 concentration levels in the atmosphere.[1] One option to mitigate the emission of CO_2 is to capture it from emission sources, store it in the ocean or underground, or use it for enhanced oil and coal bed methane recovery. Before CO_2 can be sequestered, it must be separated and concentrated from a flue gas with a low CO_2 concentration. There are a variety of approaches to CO_2 separation from other flue gas components, such as gas absorption, membranes, cryogenic distillation, gas adsorption and others, each with their own pros and cons.[2] Currently, absorption based technologies are commercially utilized for CO_2 capture, in which different kinds of amines are used as solvents for absorbing CO_2 from flue gas. Typical energy requirements for the leading absorption technologies are quite high, ranging from 765 to 950 kWh tonne^{-1} CO_2 captured (excluding energy requirement for CO_2 compression).[3] Recent developments have shown pressure/vacuum swing adsorption to be a promising option for separating CO_2 at high purity and with low power requirements. PSA processes have been widely applied for the removal of CO_2 from various feed mixtures, such as CO_2 in the steam reformer off-gas, natural gas, and flue gas.[4] They are also commercially used to remove trace amounts of CO_2 from air.[5] In these commercial PSA cycles, the weakly adsorbed (or light) component in the mixture is the desired product and enriching the strongly adsorbed (or heavy) component (in this case, CO_2) is not a concern. On the other hand, for CO_2 sequestration, it is necessary to concentrate CO_2 to a high purity to reduce the compression and the transportation cost. Moreover, safety and environmental issues are the additional reasons for concentrating CO_2 to a high purity.

Typically adsorbents preferentially adsorb CO_2 from a flue gas mixture, consequently making it a heavy product. The conventional PSA cycles are inappropriate for concentrating heavy product because the light product purge step (or the light reflux step) in these cycles uses a portion of the light product gas, which necessarily dilutes the heavy component in the heavy product stream. As a result, a pure light component is easy to attain from such cycles, but not a pure heavy component. Thus, it is necessary to develop PSA processes specifically targeted to obtain pure strongly adsorbed component, CO_2 in this case.

Because the product purity of the heavy component is limited by the gas mixture occupying the void spaces in the bed, its purity can be increased by displacing the gas mixture in the void spaces with a pure heavy product gas. For instance, for the separation of N_2-CO_2 mixture, the displacement can be accomplished by purging the bed with CO_2 after the adsorption step in the PSA cycle. Hence, to obtain a pure heavy product gas, a heavy product pressurization step or a heavy reflux step is necessary in the cycle, similar to a light product pressurization step or a light reflux step in the conventional PSA cycles. This idea was first suggested in a patent by Tamura,[6] and has been incorporated in most of the PSA cycles that have been suggested in the literature for high purity CO_2 separation from flue gas.

A fairly comprehensive review of the previous studies on PSA cycles for concentrating CO_2 from flue gas is presented in the next section. This review highlights the difficulties associated with choosing one PSA cycle over another for a given application. From these studies, it is not clear why a particular cycle was chosen or one performed better than other configurations. More importantly, the review shows that so far no systematic algorithm or method has been developed in the literature to design and evaluate a PSA cycle configuration to obtain a pure light or a heavy product or both simultaneously. Therefore, our objective is to present a systematic approach to develop, evaluate, and optimize PSA cycles for CO_2 capture.

In this article, we present an optimization-based framework to generate optimal PSA cycles from a 2-bed PSA superstructure, and apply the approach to develop optimal configurations to separate CO_2 from a flue gas mixture. The cycles are optimal because they are realized after solving an optimal control problem. It is worth noting that in this work, we consider a detailed partial differential algebraic equation (PDAE) based mathematical model, with the cyclic steady state condition, for the optimization problem and the model accommodates detailed adsorption physics. The PDAE-based model is completely discretized in both spatial and time domains, and the resulting large-scale nonlinear programming problem is solved using an interior point solver. "PSA Superstructure" section describes the optimal control framework formulated to realize different operating steps in a PSA cycle. "PSA Model and Solution Methodology" section describes the PSA model equations and the solution strategy while the subsequent section describes the case studies. Concluding remarks are outlined in the final section.

Literature Review

Since 1992, when the Japanese power industry started investigating flue gas CO_2 removal using gas adsorption,[7–11] a multitude of PSA/VSA cycles have been developed in the literature to produce pure CO_2 from a flue gas mixture. We provide a summary of these studies in Table 1. In this table, y_f is the CO_2 % in feed, while p_{CO_2} and r_{CO_2} are CO_2 purity and recovery in the heavy product stream, respectively, and P_l is the vacuum/low pressure used to extract CO_2 at high purity. The terminology for various operating steps in a cycle is adopted from Reynolds et al.[12] Most of these studies

Table 1. PSA Cycles Suggested in the Literature for Post-Combustion CO_2 Separation

PSA Cycle Configuration	Operating Step Sequence*	Ads†	y_f (%)	p_{CO_2} (%)	r_{CO_2} (%)	P_l (kPa)	Feed throughput (kg-mol h^{-1})	References
5-bed 5-step	F,HR,CnD,LR,LPP	HTlc	15	72	82	11.49	0.001	12‡
5-bed 5-step	F,HR,CnD,LR,LPP	HTlc	15	76	49	11.49	0.003	12‡
4-bed 4-step	F,HR,CnD,LPP	HTlc	15	83	17	11.49	0.001	12‡
5-bed 5-step	F,HR,CnD,LR,LPP	HTlc	15	98.7	98.7	11.64	0.00052	13‡
5-bed 5-step	F+R,HR,CnD,LR,LPP	HTlc	15	98.6	91.8	11.64	0.00052	13‡
4-bed 4-step	F,HR,CnD,LPP	HTlc	15	99.2	15.2	11.64	0.006	13‡
4-bed 4-step	F+R,HR,CnD,LPP	HTlc	15	99.2	15.2	11.64	0.006	13‡
4-bed 4-step	LPP,F+R,HR,CnD	AC	17	99.9	68	10.13	16.19	14‡
3-bed 8-step	FP,F,CoD,R,N,HR,CnD,N	13X	16	99	45	6.67	0.049	15
4-bed 8-step	FP,F,HR,LEE,CnD,LR,LEE,N	NaX	13	95	50	10	1.116	16‡,§
2-bed 4-step	FP,F,CnD,LR	13X	10	70	68	4	0.331	17‡
2-bed 6-step	LEE,FP,F,LEE,CnD,LR	13X	10	82	57	6.67	0.331	17‡
3-bed 5-step	FP,F,HR,CnD,LR	13X	10	83	54	6.67	0.331	17‡
2-bed 4-step	FP,F,CnD,LR	13X	8.3	78	50	101.3	0.004	18§
3-bed 8-step	FP,F,CoD,LEE,HPP,HR,CnD,LEE	AC	17	99.8	34	10.13	0.027	19‡,§
3-bed 7-step	FP,F,LEE,HR,N,CnD,LEE	AC	13	99	55	10.13	0.204	20‡,§
3-bed 8-step	FP,F,CoD,LEE,HPP,HR,CnD,LEE	13X	13	99.5	69	5.07	0.025	21‡,§
2-bed 4-step	HPP,FP,CoD,CnD	13X	20	48	94	5.07	–	22
2-bed 5-step	HPP,FP,F,CoD,CnD	13X	20	43	88	5.07	–	22
3-bed 4-step	LPP,F,CnD,LR	13X	20	58	75	5.07	–	22
3-bed 6-step	LPP,FP,F,HR,CoD,CnD	13X	20	63	70	5.07	–	22
2-bed 4-step	FP,F,CnD,LR	13X	15	72	94	90	30.35	23
1-bed 4-step	FP,F,CoD,CnD	13X	15	90	94	70	1.741	23
2-bed 4-step	LPP,F,CnD,LR	13X	15	52	66	10	0.007	24§
3-bed 5-step	LPP,F,HR,CnD,LR	13X	15	83	66	10	48.57	24§
3-bed 6-step	F,LEE,CnD,LEE	13X	12	83	60	4	0.193	25‡,§
3-bed 9-step	F,LEE,HR,CnD,LEE	13X	12	95	60	5	0.193	26‡,§
3-bed 9-step	F,LEE,I,LEE,CnD,LEE,FP	13X	12	92.5	75	3	0.327	27‡

*Cycle-step legend: CnD, counter-current depressurization; CoD, co-current depressurization; FP, feed pressurization; F, feed or adsorption; HPP, heavy product pressurization; HR, heavy reflux; LEE, light end equalization; LPP, light product pressurization; LR, light reflux; N, null or idle; R, recycle.
†Adsorbent legend: HTlc, K-promoted Hydrotalcite; NaX, 13X, molecular sieve zeolites; AC, activated carbon.
‡Studies with experimental results.
§Multicomponent study.

are bench-scale and deal with extremely small feed throughput.

Ritter and co-workers have studied numerous PSA cycles for CO_2 capture from a feed at high temperature using K-promoted Hydrotalcite as the adsorbent.[12,28,29] They have emphasized the importance of including heavy reflux step to obtain heavy product at a high purity. They compared seven different 4-bed 4-step, 4-bed 5-step, and 5-bed 5-step cycle configurations with and without heavy reflux step. In another work,[13] they analyzed nine different PSA configurations and achieved better purities and recoveries for CO_2, although, at an extremely small feed throughput. Kikkinides et al.[14] studied a 4-bed 4-step vacuum swing process and improved CO_2 purity and recovery by allowing significant breakthrough of CO_2 from the light end of the column undergoing heavy reflux, and then, recycling the effluent from this light end back to the column with the feed. Chue et al.[15] compared activated carbon and zeolite 13X using a 3-bed 9-step VSA process. They suggested that despite a high heat of adsorption of CO_2, zeolite 13X is better because of its higher working capacity, lower purge requirement, and higher equilibrium selectivity. PSA cycle sequences that took advantage of both light and heavy reflux steps were explored by Takamura et al.[16] and Park et al.[17] Takamura et al. studied a 4-bed 8-step VSA process whereas Park et al. analyzed three different cycle configurations for VSA processes. Although the pure CO_2 rinse step and the equalization step in the 3-bed 5-step cycle improved their CO_2 purity and recovery, it didn't decrease their power requirements, which were 106.91 kWh $tonne^{-1}$ CO_2 captured for the 2-bed 6-step cycle, and 147.64 kWh $tonne^{-1}$ CO_2 captured for the 3-bed 5-step cycle. Though the power consumption was quite low, the feed throughput of 0.331 kg-mol h^{-1} was also on the lower side. The conventional 2-bed 4-step Skarstrom cycle was also studied by Gomes et al.,[18] in which they didn't apply vacuum to recover CO_2. Their work also showed that the light reflux step itself is not sufficient to obtain pure heavy component.

Na et al.[19,20] and Choi et al.[21] studied 3-bed 8-step and 3-bed 7-step VSA configurations experimentally as well as numerically. Light reflux step was not used for any of these configurations, whereas heavy reflux was used in all of them. The 2-bed cycles of Chou and Chen[22] did not use any kind of reflux steps whereas the 3-bed cycles used both light and heavy reflux steps. The 2-bed cycles were unconventional as flow reversal was implemented in between the pressurization and depressurization steps. Similarly, the 3-bed 6-step cycle incorporated an unusual co-current light product pressurization step. They couldn't go beyond 63% CO_2 purity, which was achieved using the 3-bed 6-step cycle. Ko et al.[23] optimized a 2-bed 4-step PSA process to minimize power consumption, and a 1-bed 4-step fractionated VPSA process to increase CO_2 purity to

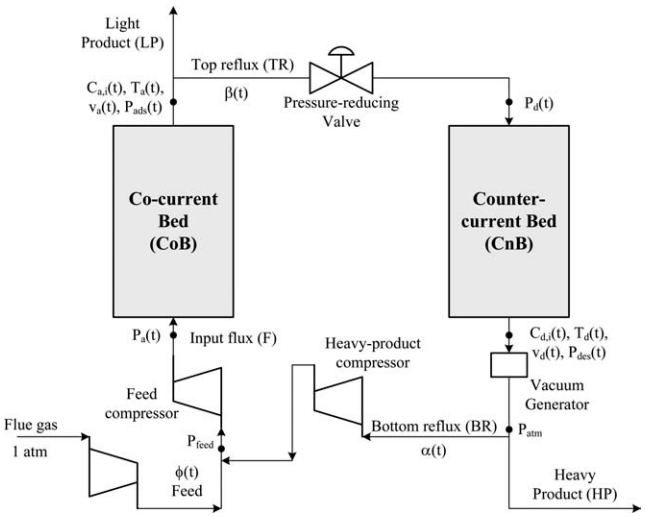

Figure 1. A 2-bed PSA superstructure.

90% and recovery to 94%. Grande et al.[24] studied a classical Skarstrom cycle with light product pressurization and a 3-bed 5-step process which included a pure CO_2 rinse step after the adsorption step. Their scale-up study showed that a purity of 83% and a recovery of 66% is possible with the 3-bed 5-step process at a much higher feed throughput of 48.57 kg-mol h^{-1}.

Webley and co-workers[25–27,30] have done an extensive research in the field of CO_2 separation by adsorption. Chaffee et al.[25] and Zhang et al.[26] studied two different VSA processes. For a low feed throughput of 0.193 kg-mol h^{-1} for both the cycles, they achieved a low power consumption of 192 kWh $tonne^{-1}$ CO_2 captured for the 3-bed 6-step and 240 kWh $tonne^{-1}$ CO_2 captured for the 3-bed 9-step cycle. Xiao et al.[27] studied a similar 3-bed 9-step cycle and were able to increase CO_2 recovery to 75%. In another study, Zhang and Webley[30] compared numerous VSA cycle configurations, and showed that CO_2 purity can be increased by particularly incorporating heavy reflux and equalization steps.

Although this review offers some trends and guidelines, a fully systematic methodology is still required to design PSA cycle configurations. Zhang and Webley[30] outlined an approach for cycle development by understanding the roles of individual operating steps and adsorption fronts. However, they identified optimal configurations with the help of a pre-decided set of operating steps and a simplified mathematical model. Chiang[31] and Smith et al.[32] described heuristic-based and mixed integer nonlinear programming (MINLP) based formulations, respectively, to determine minimum number of beds required to design a PSA process around a given sequence of operating steps, but didn't discuss how the steps should be chosen. Smith and Westerberg[33,34] also gave a 3-step scenario to design an industrial PSA system, but again with a known sequence of operating steps. In contrast, this work presents a novel superstructure-based approach to obtain optimal sequence of operating steps in a PSA cycle without any assumption on the kinds of steps that should be included within the cycle. As discussed in the next section, this approach relies on the formulation of an optimal control problem.

PSA Superstructure

With the development of optimization strategies for process synthesis, it is natural to consider a superstructure based approach to design PSA processes. Figure 1 shows the 2-bed PSA superstructure developed in this work. It has a co-current bed (CoB) and a counter-current bed (CnB) that determine co-current and counter-current operating steps in the cycle, respectively. We consider only two beds to ensure that the direction of the flow, and thus, the superficial velocity, remains co-current for CoB and counter-current for CnB. This strategy avoids flow reversals in the bed, as well as a possible network of bed connections with embedded logical conditions to realize different operating steps. This superstructure is consistent with the concept of unibed models,[35] *where no more* than *two beds interact* at the same time, and the steps can be grouped into *adsorbing steps* and *desorbing steps*. Consequently, it can accomplish a wide variety of these operating steps with just a single bed connection, as shown in Figure 1. Furthermore, this helps to avoid discrete variables and uses only continuous variables for the optimization problem.

The superstructure is designed to get the light product from the upper end (light end) of CoB and heavy product from the lower end (heavy end) of CnB. The time dependent variables $\beta(t)$ and $\alpha(t)$ determine the fraction of the light product and the heavy product streams that go into the top and the bottom reflux, respectively. The flue gas, coming at atmospheric pressure, is compressed to P_{feed} to increase the feed throughput. The time dependent feed fraction $\phi(t)$ determines the feeding strategy. For CoB, pressure is specified at the light end by P_{ads}, whereas the pressure at the other end P_a is determined from the pressure drop in this bed. The velocity v_a, concentration for ith component $C_{a,i}$, and temperature T_a at the light end are determined from the outlet flux. Similarly, for CnB, pressure is specified at the heavy end by P_{des}, while $C_{d,i}$, T_d and v_d are obtained from the output flux, and P_d is obtained from the pressure drop. The superstructure also incorporates compressors and valves to account for different pressure levels in the beds, and a vacuum generator to extract the strongly-adsorbed component.

It is possible to accomplish a wide variety of different operating steps of a PSA process by varying the control variables $\alpha(t)$, $\beta(t)$, $\phi(t)$, $P_{ads}(t)$, and $P_{des}(t)$, as shown in Figure 2. As a consequence, the temporal profiles of $\alpha(t)$, $\beta(t)$, $\phi(t)$, $P_{ads}(t)$ and $P_{des}(t)$ result into a sequence of operating steps, thus generating a PSA cycle. For instance, the profiles of $\alpha(t)$, $\beta(t)$, and $\phi(t)$, shown in Figure 3, translate into the classical 2-bed 4-step Skarstrom cycle (FP,F,CnD,LR).[36] CoB generates pressurization (FP) and feed (F) steps, while CnB simultaneously generates depressurization (CnD) and light reflux (LR) steps. Thus, the overall cycle includes these four steps (FP,F,CnD,LR). In an actual 2-bed PSA unit, after performing its steps, CoB will follow the steps of CnB and vice-versa. However, in the mathematical framework, this is realized by giving final conditions of CoB as the initial conditions for CnB and vice-versa, thus modeling the true 2-bed behavior. This multibed approach is described in detail in Jiang et al.[37] An optimal sequence of operating steps, along

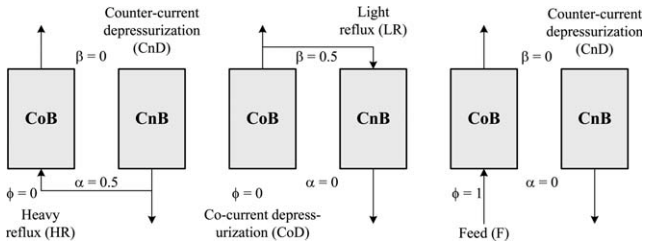

Figure 2. Realization of different operating steps by varying control variables.

with other decision variables, such as cycle time, individual step times, and bed dimensions, is obtained by solving the following optimization problem.

$$\begin{aligned}
&\min \\
&\quad \Phi(z(x,t_f), y(x,t_f), \alpha(t_f), \beta(t_f), \phi(t_f), z(x,0), p) \\
&\text{s.t.} \\
&\mathrm{f}\left(\frac{\partial z}{\partial t}, \frac{\partial z}{\partial x}, z(x,t), y(x,t), \alpha(t), \beta(t), \phi(t), P_{\mathrm{ads}}(t), P_{\mathrm{des}}(t), z(x,0), p\right) \\
&\qquad = 0 \\
&\quad z_{\mathrm{CoB}}(x,0) = z_{\mathrm{CnB}}(x,t_f), \quad z_{\mathrm{CnB}}(x,0) = z_{\mathrm{CoB}}(x,t_f) \\
&\quad s(z(x,t), y(x,t), \alpha(t), \beta(t), \phi(t), p) = 0 \\
&\quad g(z(x,t), y(x,t), \alpha(t), \beta(t), \phi(t), p) \le 0 \\
&\quad 0 \le \alpha(t), \beta(t), \phi(t) \le 1 \\
&\quad b_{\mathrm{L}} \le (P_{\mathrm{ads}}, P_{\mathrm{des}}, p) \le b_{\mathrm{U}} \qquad (1)
\end{aligned}$$

Here, Φ is the objective function related to overall power consumption, component purity or recovery. It can depend upon differential variables $z(x, t)$, algebraic variables $y(x, t)$, control variables $\alpha(t)$, $\beta(t)$, and $\phi(t)$, initial conditions z$(x, 0)$ and other decision variables p. The first equation represents the PDAE-based model for the PSA system, while the second equation is the cyclic steady state (CSS) condition (see Table 2). As mentioned before, the CSS condition is implemented by giving final conditions of CoB as the initial condition for the CnB and vice versa. Additional constraints for the optimization problem are given by the algebraic equations s and the inequalities g. The control variables $\alpha(t)$, $\beta(t)$, and $\phi(t)$ are fractions bounded between 0 and 1. Other control variables, $P_{\mathrm{ads}}(t)$ and $P_{\mathrm{des}}(t)$, and decision variables p are bounded between their respective bounds b_{L} and b_{U}.

It is important to note that although optimal 2-bed PSA configurations are construed from the optimal profiles of $\alpha(t)$, $\beta(t)$, $\phi(t)$, $P_{\mathrm{ads}}(t)$, and $P_{\mathrm{des}}(t)$, multibed cycles (with more than two beds) follow immediately from these solutions. These are generated by staggering the steps over multiple beds and ensuring that a bed with a product flow step occurs at all points in time.

PSA Model and Solution Methodology

Model equations

We consider a detailed PDAE-based mathematical model for the optimal control problem. The model is fairly general and can also be extended beyond the following assumptions.

(1) All of the gases follow the ideal gas law.

(2) There are no radial variations in temperature, pressure, and concentrations of the gases in the solid and the gas phase.

(3) The gas and the solid phases are in thermal equilibrium and bulk density of the solid phase remains constant.

(4) Pressure drop along the bed is calculated by the Ergun equation.

(5) The adsorption behaviors are described by the dual-site Langmuir isotherm. This monolayer-based isotherm has the ability to accurately capture linear behavior at low pressures, a requirement for thermodynamic consistency in any physical adsorption system.[38]

(6) The adsorption rate is approximated by the linear driving force (LDF) expression. Sircar and Hufton[39] demonstrated that the LDF model is sufficient to capture the kinetics of adsorption because the estimation of the separation performance of an adsorptive process requires several sets of averaging of kinetic properties and the effect of local characteristics are lumped during integration.

On the basis of the above assumptions, the mathematical model for the PSA process is listed in Table 2. Here, we consider a lumped mass transfer coefficient for the LDF equation. Since a smaller magnitude of U_{A} makes energy balance a weak function of the ambient temperature, T_{w} is assumed constant. As a convention, flow in the counter-

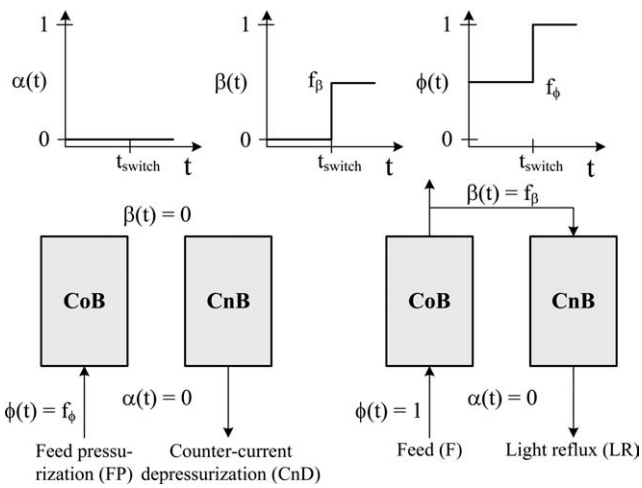

Figure 3. Realization of 4-step Skarstrom cycle from the superstructure.

Table 2. PSA Model Equations

Component mass balance

$$\varepsilon_b \frac{\partial C_i}{\partial t} + (1-\varepsilon_b)\rho_s \frac{\partial q_i}{\partial t} + \frac{\partial (vC_i)}{\partial x} = 0 \qquad i \in \{\mathrm{L, H}\} \tag{2}$$

LDF equation

$$\frac{\partial q_i}{\partial t} = k_i (q_i^* - q_i) \qquad i \in \{\mathrm{L, H}\}) \tag{3}$$

Energy balance

$$\left(\varepsilon_b \sum_i C_i (C_{pg}^i - R) + \rho_b C_{ps}\right) \frac{\partial T}{\partial t} - \rho_b \sum_i \Delta H_i^{\mathrm{ads}} \frac{\partial q_i}{\partial t} + \frac{\partial (vh)}{\partial x} + U_A (T - T_w) = 0 \tag{4}$$

$$C_{pg}^i = a_c^i + b_c^i T + c_c^i T^2 + d_c^i T^3 \qquad i \in \{\mathrm{L, H}\}$$

$$h = \sum_i \left(C_i \int C_{pg}^i \, \mathrm{d}T \right)$$

Dual-site Langmuir Isotherm

$$q_i^* = \frac{q_{1i}^s b_{1i} C_i RT}{1 + \sum_{j \in \{\mathrm{L,H}\}} b_{1j} C_j RT} + \frac{q_{2i}^s b_{2i} C_i RT}{1 + \sum_{j \in \{\mathrm{L,H}\}} b_{2j} C_j RT} \qquad i \in \{\mathrm{L, H}\} \tag{5}$$

$$q_{mi}^s = k_{mi}^1 + k_{mi}^2 T \qquad b_{mi} = k_{mi}^3 \exp\left(\frac{k_{mi}^4}{T}\right) \qquad i \in \{\mathrm{L, H}\} \qquad m = 1, 2$$

Ergun equation

$$-\frac{\partial P}{\partial x} = \frac{150\mu(1-\varepsilon_b)^2}{d_p^2 \varepsilon_b^3} v + \frac{1.75}{d_p} \left(\frac{1-\varepsilon_b}{\varepsilon_b^3}\right) \left(\sum_i M_w^i C_i\right) v|v| \tag{6}$$

Ideal gas equation

$$P = RT \sum_i C_i \tag{7}$$

Bed Connection equation (See Figure 1)

$$F_i(t) = \phi(t) v_{\mathrm{feed}} C_{\mathrm{feed},i} + \alpha(t)(-v_d(t)) C_{i,d}(t) \qquad i \in \{\mathrm{L, H}\} \tag{8}$$

$$\mathrm{TR}_i(t) = \beta(t) v_a(t) C_{a,i}(t) \qquad i \in \{\mathrm{L, H}\} \tag{9}$$

$$\mathrm{LP}_i(t) = (1-\beta(t)) v_a(t) C_{a,i}(t) \qquad i \in \{\mathrm{L, H}\} \tag{10}$$

$$\mathrm{BR}_i(t) = \alpha(t)(-v_d(t)) C_{d,i}(t) \qquad i \in \{\mathrm{L, H}\} \tag{11}$$

$$\mathrm{HP}_i(t) = (1-\alpha(t))(-v_d(t)) C_{d,i}(t) \qquad i \in \{\mathrm{L, H}\} \tag{12}$$

Cyclic Steady State (CSS) condition for beds CoB and CnB

$$\begin{aligned} z_{\mathrm{CoB}}(x,0) &= z_{\mathrm{CnB}}(x, t_f), \; z_{\mathrm{CnB}}(x,0) = z_{\mathrm{CoB}}(x, t_f), \\ z(x,t)^T &= [C_L(x,t), C_H(x,t), q_L(x,t), q_H(x,t), T(x,t)] \end{aligned} \tag{13}$$

current bed is considered negative and a minus sign is used for v_d. Since the bed model is based on fluxes, the feed throughput and the bed diameter can be adjusted as long as the specified feed flux is achieved and the model assumptions are not violated. The following equations are used to evaluate the performance variables.

$$\text{purity}_{\text{L}} = \frac{\int (1-\beta(t)) v_{\text{a}}(t) C_{\text{a,L}}(t) dt}{\int (1-\beta(t)) v_{\text{a}}(t) \sum_i C_{\text{a},i}(t) dt} \tag{14a}$$

$$\text{purity}_{\text{H}} = \frac{\int (1-\alpha(t))(-v_{\text{d}}(t)) C_{\text{d,H}}(t) dt}{\int (1-\alpha(t))(-v_{\text{d}}(t)) \sum_i C_{\text{d},i}(t) dt} \tag{14b}$$

$$\text{recovery}_{\text{L}} = \frac{\int (1-\beta(t)) v_{\text{a}}(t) C_{\text{a,L}}(t) dt}{\text{Q}_{\text{feed,L}}} \tag{14c}$$

$$\text{recovery}_{\text{H}} = \frac{\int (1-\alpha(t))(-v_{\text{d}}(t)) C_{\text{d,H}}(t) dt}{\text{Q}_{\text{feed,H}}} \tag{14d}$$

$$\text{Q}_{\text{feed},i} = \int \phi(t) v_{\text{feed}} C_{\text{feed},i}\, dt \qquad i \in \{\text{L, H}\} \tag{14e}$$

Here, Q_{feed} is the feed flux. The total power consumption, given by the following equations, is the sum of the work done by the compressors and the vacuum generator.

$$\begin{aligned} W_{\text{total}} = & \int \frac{\gamma R T_{\text{d}}}{\gamma - 1} \left[\frac{\sum_i \left(\phi(t) v_{\text{feed}} C_{\text{feed},i} + \alpha(t)(-v_{\text{d}}) C_{\text{d},i} \right)}{\eta_{\text{c}}} \left(\left(\frac{P_{\text{a}}}{P_{\text{feed}}} \right)^{\frac{\gamma-1}{\gamma}} - 1 \right) \right. \\ & + \frac{\sum_i \alpha(t)(-v_{\text{d}}) C_{\text{d},i}}{\eta_{\text{h}}} \left(\min \left\{ \left(\frac{P_{\text{feed}}}{P_{\text{atm}}} \right)^{\frac{\gamma-1}{\gamma}}, \left(\frac{P_{\text{feed}}}{P_{\text{des}}} \right)^{\frac{\gamma-1}{\gamma}} \right\} - 1 \right) \\ & \left. + \frac{\sum_i (-v_{\text{d}}) C_{\text{d},i}}{\eta_{\text{v}}} \max \left\{ 0, \left(\left(\frac{P_{\text{atm}}}{P_{\text{des}}} \right)^{\frac{\gamma-1}{\gamma}} - 1 \right) \right\} \right] \\ & + \frac{\gamma}{\gamma - 1} \frac{\phi(t) v_{\text{feed}} P_{\text{feed}}}{\eta_{\text{fg}}} \left(\left(\frac{P_{\text{feed}}}{P_{\text{atm}}} \right)^{\frac{\gamma-1}{\gamma}} - 1 \right) dt \end{aligned} \tag{15a}$$

$$\text{Power} = \frac{W_{\text{total}}}{\int (1-\alpha(t)) v_{\text{d}}(t) C_{\text{d,H}}(t) dt} \tag{15b}$$

Here, the max function ensures that the work done by the vacuum generator is zero when P_{des} is greater than atmospheric pressure P_{atm}. Similarly, since the vacuum generator discharges heavy reflux at P_{atm}, the min operator ensures a proper upstream pressure for the heavy product compressor. Since min or max operators introduce nondifferentiability, the following smoothing approximations are adopted.[40] A value of 0.01 is used for ε in the following equations.

$$\min(f_1(x), f_2(x)) = f_1(x) - \max(0, f_1(x) - f_2(x)) \tag{16a}$$

$$\max(0, f(x)) = 0.5 \left(f(x) + \sqrt{f(x)^2 + \varepsilon^2} \right) \tag{16b}$$

Solution strategy

We adopt a complete discretization approach to solve the system of PDAEs in Table 2. The PDAEs are converted into a set of algebraic equations by discretizing the state and the control variables both in space and time. As a result, the PDAE-constrained optimal control problem (Eq. 1) gets converted into a large-scale nonlinear programming (NLP) problem. One of the advantages of this approach is that it directly couples the solution of the PDAE system with the optimization problem. The model equations are solved only once at the optimum and the excessive computational effort of getting intermediate solutions is avoided.[41] However, the performance of this approach substantially depends upon the optimization solver, and therefore, it is crucial to choose an efficient NLP solver. Hence, we use the state-of-the-art NLP solver IPOPT 3.4 for our case studies. This interior point solver uses a barrier method to handle inequalities and exact second derivative information for faster convergence to the optimum.[42]

Hyperbolic PDAEs in Table 2 are characterized by steep adsorption fronts in spatial domain for concentrations and temperature. To capture such steep profiles, it is important to use a spatial discretization method which not only avoids physically unrealistic oscillations, but also is suited to model conservative properties.[43,44] Therefore, a first-order finite volume method is applied for spatial discretization. The differential algebraic equations (DAEs), resulting from spatial discretization, are then converted into a set of algebraic equations by applying orthogonal collocation on finite elements in temporal domain. A Radau collocation scheme is considered because it allows us to set constraints at the ends of the finite elements.[45] A 3-point collocation scheme is used for state variables while control variables are considered to be piecewise constant. We also consider a moving finite element strategy in which the length of each temporal finite element is considered a decision variable in the optimization problem. With moving finite elements, it is possible to locate optimal breakpoints of the control variables with variable element lengths. Appropriate bounds are imposed on the variable element lengths of each finite element to guarantee the accuracy of the discretization.

Since a large number of spatially discretized nodes are required to capture steep adsorption fronts, such fine spatial discretization leads to a large set of DAEs which after temporal discretization leads to a very large set of algebraic equations, that becomes expensive to solve. Moreover, in the absence of any error checking mechanism for temporal integration, pre-determined temporal discretization may lead to inaccurate profiles due to insufficient number of finite elements. Although a large number of elements will improve the accuracy, it will again make the problem computationally challenging to solve. Hence, to get the solution in a reasonable amount of time, we consider only 20 spatial finite volumes and around 25 temporal finite elements for the optimization problem. Because such a small number of nodes can cause inaccuracies to creep in the NLP solution obtained from IPOPT, verification of this solution with an accurate dynamic simulation is essential. Thus, we carry out dynamic simulations in MATLAB[46] at the optimal values obtained from IPOPT. The DAE system obtained after applying method of lines is integrated in MATLAB at the optimal values of the decision variables. The profiles and performance variables obtained from MATLAB are then compared with those obtained from IPOPT.

Finally, because all of the control variables appear linearly, problem (1) is a singular optimal control problem. Such problems are characterized by shallow response surfaces. Moreover, the Euler-Lagrange equations obtained after applying the maximum principle to (1) are high index in nature and ill-conditioned. Consequently, a fine discretization

of the control variable profiles also leads to an ill-conditioned problem with solutions often characterized by oscillations that do not subside with increasing mesh refinement.[47] As a result, we adopt a relatively coarse discretization of the control profiles. Although this will lead to suboptimal (but generally quite good) solutions, it also helps to regularize the solution profiles and ameliorate the singular nature of the optimal control problem.

Case Studies and Computational Results

In this section, we consider a post-combustion CO_2 separation system that illustrates the superstructure methodology to obtain optimal PSA cycles. We consider an 85%–15% N_2 -CO_2 feed mixture which is a typical composition of a post-combustion flue gas stream. As an initial study, the focus is on a binary feed mixture. A multicomponent feed mixture also having water, oxygen and other trace components will be considered in the future extensions of this work. We assume that the flue gas enters at a temperature of 310 K, and a maximum velocity (v_{feed}) of 50 cm s^{-1}. The inlet pressure P_{feed} varies with the case studies. Zeolite 13X is chosen as the adsorbent to separate CO_2; Chue et al.[15] suggested it to be a preferable adsorbent over others for this separation system. The adsorbent properties for 13X and other model parameters are listed in Table 3.[23] We consider three different cases to explore different facets of the superstructure approach. The first case study optimizes the 2-bed 4-step Skarstrom configuration, obtained after fixing the control variables in the superstructure, and shows the ineffectiveness of such traditional cycles for high-purity CO_2 separation. The second case then finds an optimal PSA configuration which separates CO_2 at a high purity and recovery. Finally, in the third case, we find an optimal configuration which achieves high-purity separation with minimal power requirements.

Table 3. Zeolite 13X Properties and Model Parameters[23]

Parameter	Value
Bulk porosity (ε_b)	0.34
Particle diameter (d_p)	0.002 m
Adsorbent density (ρ_s)	1870 kg m^{-3}
Bulk density (ρ_b)	1234.2 kg m^{-3}
Heat capacity of solid (C_{ps})	450.54 J kg^{-1} K^{-1}
Heat transfer coefficient (U_A)	926.7 J m^{-3} s^{-1} K^{-1}
Gas viscosity (μ)	1.7857×10^{-5} kg m^{-1} s^{-1}
Gas constant (R)	8.314 J g-mol^{-1} K^{-1}
Mass transfer coefficient (k)	$CO_2 = 0.1631$ s^{-1}
	$N_2 = 0.2044$ s^{-1}
Heat of adsorption (ΔH^{ads})	$CO_2 = 23011.14$ J g-mol^{-1}
	$N_2 = 14452.72$ J g-mol^{-1}
Ambient temperature (T_w)	298 K

Isotherm parameters	CO_2	N_2
k_1^1	2.817269	1.889581
k_1^2	-3.51×10^{-4}	-2.25×10^{-4}
k_1^3	2.83×10^{-9}	1.16×10^{-9}
k_1^4	2598.203	1944.606
k_2^1	3.970888	1.889581
k_2^2	-4.95×10^{-3}	-2.25×10^{-4}
k_2^3	4.41×10^{-9}	1.16×10^{-9}
k_2^4	3594.071	1944.606

Case 1: Optimization with a conventional configuration

First, we explore the potential of the conventional 2-bed 4-step Skarstrom cycle for post-combustion CO_2 capture. For this, we fix the profiles of $\alpha(t)$, $\beta(t)$, and $\phi(t)$ over time, as shown in the Figure 3. While f_β is chosen as 0.3 , f_ϕ before t_{switch} is fixed to 0.35. This ensures that the superficial velocity is close to zero towards the light end of CoB during the FP step. In this case, P_{ads} and P_{des} remain constant for the entire cycle. The inlet pressure P_{feed} is fixed to 300 kPa, as considered by Gomes et al.[18] as well.

With this configuration we maximize CO_2 recovery. Since the lack of any heavy reflux step in the configuration may not enable a high purity separation, a relatively low value of 40% is chosen for the lower bound on CO_2 purity. Besides P_{ads} and P_{des}, we also consider bed length BLen, and cycle time T_c as decision variables. Since a moving finite element strategy is adopted, the length of each finite element is also considered as an optimization variable. Because none of the decision variables are functions of time, the optimal control problem (1) becomes a dynamic optimization problem, which becomes the following NLP after discretizing PDAEs in both space and time.

$$\max \quad \text{CO_2 recovery (from Eq. 14d)}$$

$$\text{s.t.}$$

$$c(w) = 0 \text{ (fully discretized Eqs. 2–13)} \tag{17a}$$

$$\text{CO_2 purity} \geq 0.4 \text{ (from Eq. 14b)} \tag{17b}$$

$$P_{ads} \geq P_d \tag{17c}$$

$$P_{des} \leq P_{feed} \tag{17d}$$

$$P_a \geq P_{feed} \tag{17e}$$

$$1\,\text{m} \leq \text{BLen} \leq 6\,\text{m} \tag{17f}$$

$$20\,\text{s} \leq T_c \leq 2400\,\text{s} \tag{17g}$$

$$101.32\,\text{kPa} \leq P_{ads} \leq 1000\,\text{kPa} \tag{17h}$$

$$P_{des} \geq 10\,\text{kPa} \tag{17i}$$

Here w and $c(w) = 0$ represent the set of completely discretized variables and model equations, respectively. Constraint (17c) ensures that the pressure always drops around the pressure reducing valve in the superstructure. Similarly, constraints (17d) and (17e) ensure that the gas is never expanded by the heavy gas and the feed compressors, respectively. The rest of the inequalities are bounds on the decision variables.

With 24 temporal finite elements and 20 spatial finite volumes, we solved the NLP in AMPL[48] using IPOPT. Table 4 includes a summary of the optimization results. With 35,000 variables and 29 degrees of freedom, we were able to solve it to optimality in around 3 CPU h. Optimal moving finite element lengths and cycle time of 2140 s yield an optimal step time of 760 for pressurization (and depressurization) step, and 410 for feed (and light reflux) step. Such a long

Table 4. Optimization Results for Case 1

No. of variables	35022	
No. of equations	34993	
CPU time	176.94 min	
Optimal step times		
Step 1 (and 3)	760 s	
Step 2 (and 4)	410 s	
Optimal parameters	BLen = 5.51 m	T_c = 2140 s
	P_{ads} = 276.43 kPa	P_{des} = 21.75 kPa

Accuracy check	Full discretization	MATLAB verification
N_2 purity	91.25%	90.74%
N_2 recovery	85.88%	85.94%
CO_2 purity	40%	38.65%
CO_2 recovery	53.36%	50.22%

pressurization step is due to a small amount of feed during that step, which requires longer time for bed to get pressurized and CO_2 to adsorb. At the optimum, the cycle handles a feed flux of 96.4 kg-mol m^{-2} h^{-1}, which is higher than the corresponding 2-bed 4-step case studies in Table 1. At a purity of 40%, a maximum CO_2 recovery of only 53.4% was achieved. Such poor performance proves the point made in the introduction; classical cycles without heavy reflux cannot produce heavy product at high purity since a light reflux step dilutes the heavy product and decreases its purity. Table 4 also lists the MATLAB verification of the AMPL results. We considered 20 spatial finite volumes for MATLAB as well. A comparison of the purities and the recoveries indicates reasonable accuracy for the complete discretization approach.

Case 2: Cycle synthesis to maximize CO_2 recovery

Since a high-purity CO_2 separation wasn't achieved by the Skarstrom cycle, in this case we solve the optimal control problem (1) to obtain an optimal configuration which yields better performance. For this, a few modifications are essential to the optimization problem presented in the previous case. The control variables $\alpha(t)$, $\beta(t)$, and $\phi(t)$ are freed to let them achieve an optimal sequence of operating steps. The pressures P_{ads} and P_{des} are converted back to time dependent control variables. To keep this case comparable to the previous one, we fix the bed length to 5 m. A desired CO_2 purity of at least 95% is chosen. Besides this, we impose a lower bound on feed flux Q_{feed}, in the absence of which the optimizer may force the feed fraction $\phi(t)$ to zero to maximize CO_2 recovery. Finally, we add the equation for power consumption (15b) to the optimal control problem. A 72% efficiency is assumed for all the compressors and the vacuum generator unit. As in the previous case, we fix the flue gas inlet pressure P_{feed} to 300 kPa to achieve a reasonable Q_{feed}. The following large-scale NLP results after complete discretization of state and control variables in the optimal control problem.

$$
\begin{aligned}
\max \quad & CO_2 \text{ recovery (from Eq. 14d)} \\
\text{s.t.} \quad & c(w) = 0 \text{ (fully discretized Eqs. 2–13)} \\
& CO_2 \text{ purity} \geq 0.95 \text{ (from Eq. 14b)} \\
& Q_{feed,L} + Q_{feed,H} \geq 80 \,\text{kg-mol}\,\text{m}^{-2}\,\text{h}^{-1} \\
& P_{ads} \geq P_d \\
& P_{des} \leq P_{feed} \\
& P_a \geq P_{feed} \\
& 0 \leq \alpha(t_i), \beta(t_i), \phi(t_i) \leq 1 \qquad \forall t_i \\
& 20\,\text{s} \leq T_c \leq 2400\,\text{s} \\
& 101.32\,\text{kPa} \leq P_{ads}(t_i) \leq 600\,\text{kPa} \qquad \forall t_i \\
& P_{des}(t_i) \geq 50\,\text{kPa} \qquad \forall t_i
\end{aligned}
\tag{18}
$$

As in the previous case study, $c(w)$ is the set of completely discretized PDAEs with CSS condition. We choose a lower bound of 50 kPa for the vacuum generated, which is not a substantially high vacuum. Similarly, the chosen upper bound of 600 kPa for P_{ads} is also not substantially high. No bounds are specified for the purity and the recovery of nitrogen. We impose a lower bound of 80 kg-mol m^{-2} h^{-1} on the total feed flux. Because the bound is not on the feed throughput, a bigger diameter PSA bed will be able to handle much higher feed throughput and the optimal

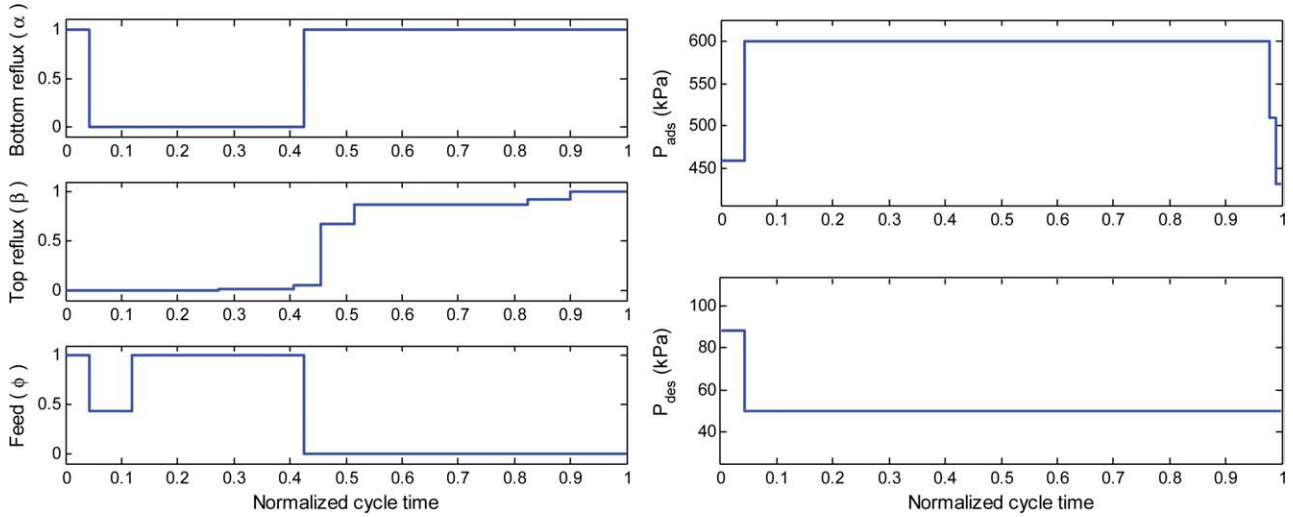

Figure 4. Optimal control profiles for Case 2.

[Color figure can be viewed in the online issue, which is available at www.interscience.wiley.com.]

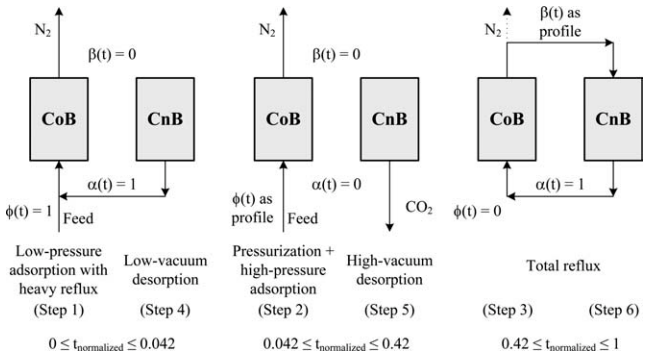

Figure 5. Optimal VSA configuration for Case 2.

configuration need not change. For instance, for a 3 m bed diameter, one PSA column will be able to handle a significantly high feed throughput of 565 kg-mol h^{-1} for the same optimal configuration. Also note that the value of 80 kg-mol m^{-2} h^{-1} is significantly higher than feed flux chosen in the literature studies in Table 1, as the focus here is to synthesize industrial scale PSA systems.

The NLP was solved in AMPL with 26 temporal finite elements and 20 spatial finite volumes. The optimal control profiles are shown in Figure 4. The profiles are drawn against cycle time normalized between 0 and 1. These profiles suggest an optimal 2-bed 6-step VSA process, illustrated in Figure 5, which can be deciphered in the following manner. The cycle starts with $\alpha(t) = 1$, $\beta(t) = 0$, and $\phi(t) =$

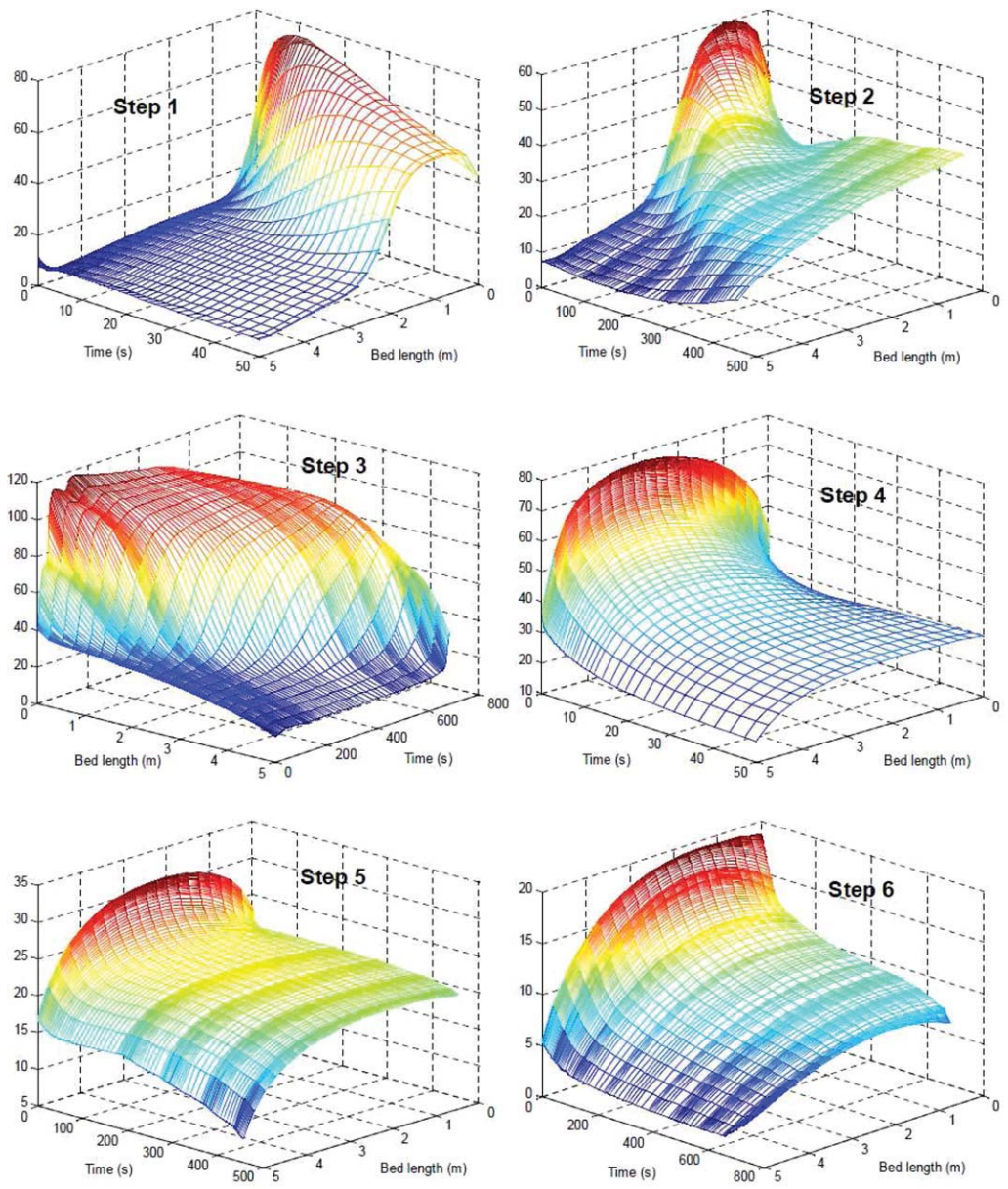

Figure 6. Gas-phase CO_2 concentration profiles for Case 2.

[Color figure can be viewed in the online issue, which is available at www.interscience.wiley.com.]

Table 5. Optimization Results for Case 2

No. of variables	50162
No. of equations	49956
CPU time	756.22 min.
Optimal step times	
Step 1 (and 4)	50 s
Step 2 (and 5)	405 s
Step 3 (and 6)	685 s
Optimal cycle time	2280 s
Feed flux	80 kg-mol m^{-2} h^{-1}
Power consumption	637.25 kWh $tonne^{-1}$ CO_2
CO_2 purity	95%
CO_2 recovery	80.09%

1. This suggests a bottom reflux from CnB to CoB and feed being fed to CoB. From the profiles of $P_{ads}(t)$ and $P_{des}(t)$, CoB operates at around 450 kPa while CnB operates at around 85 kPa during this step. Thus, we have a low-pressure adsorption step with a heavy reflux for CoB (step 1) and a low-vacuum desorption step for CnB (step 4) with desorbed CO_2 being sent as a heavy reflux from CnB to CoB. This heavy reflux joins the feed low in CO_2 concentration and enriches the adsorbed CO_2 concentration towards the heavy end of CoB. This is evident from the gas-phase CO_2 concentration profile for step 1 in Figure 6. After this step, both top and bottom reflux disappear, while $\phi(t)$ indicates continuation of the feed to CoB. CoB gets pressurized to the upper bound of 600 kPa and N_2 is withdrawn at a high pressure, while CO_2 is extracted from CnB at a vacuum of 50 kPa. This suggests a pressurization and high pressure adsorption step for CoB (step 2) and a high vacuum desorption step for CnB (step 5). The feed fraction $\phi(t)$ drops at the beginning of this step to facilitate CoB pressurization. We observe a drop in the CO_2 concentration in CoB (see step 2 in Figure 6) because of its low concentration in feed. Also, because of the application of vacuum, the gas-phase CO_2 concentration decreases sharply for both step 4 and 5, as is evident Figure 6.

Further, the pressures in the beds are held at their same respective levels, while $\alpha(t)$ becomes 1, $\beta(t)$ approaches 1, and the feed is stopped completely. Because there is no feed nor product at this time, we have a total reflux step (step 3 and 6), in which both the beds are connected to each other and a recirculation of the components occurs within the system. A small amount of N_2 is withdrawn at the beginning of this step, and is shown as a dotted line in Figure 5. During this step, nitrogen from CoB to CnB purges CO_2 out of CnB from its heavy end and enriches itself towards the light end of CnB while pushing its front. Similarly, CO_2 from CnB to CoB purges nitrogen out of CoB and enriches itself towards the heavy end of CoB and pushes its front towards the light end of CoB. Step 3 in Figure 6 confirms the movement of this CO_2 front. A decrease in $P_{ads}(t)$ and an increase in $P_{des}(t)$ towards the end of this step halts this recirculation. After the total reflux step, the co-current bed follows the steps of the counter-current bed and vice-versa. This completes the cycle.

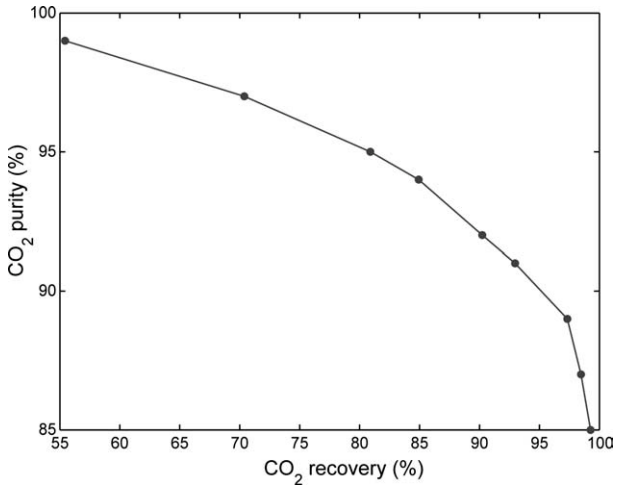

Figure 7. Purity-recovery trade-off curve for Case 2.

The optimization results for this case are summarized in Table 5. With 50,162 variables and 206 degrees of freedom, it was solved to optimality in ~12.5 CPU hours on an Intel Quad core 2.4 GHz system with 8 GB RAM. At the optimum, the feed flux attained its lower bound of 80 kg-mol m^{-2} h^{-1}. For such a high feed flux, we obtained a reasonable power consumption of 637.25 kWh $tonne^{-1}$ CO_2 captured. Also, an optimum CO_2 recovery of 80% at a purity of 95%, for such a high feed flux, is substantially better than the literature studies for post-combustion capture that deal with high feed throughput. These results confirm our assertion that steps like heavy reflux are essential for high-purity CO_2 separation.

In Table 6, we provide a validation of the optimal results obtained from AMPL with method of lines simulations in MATLAB for varying numbers of spatial finite volumes. The results from AMPL are in good agreement with those from MATLAB, and the accuracy doesn't suffer as we consider a large number of finite volumes in MATLAB. This indicates that the complete discretization approach is reasonably accurate.

Figure 7 shows a trade-off curve between CO_2 purity and recovery. We construct this curve by varying the lower bound on CO_2 purity in the NLP (18), and then maximizing

Table 6. Accuracy Validation for AMPL Results of Case 2

	AMPL Results	MATLAB Verification		
Spatial finite volumes	20	20	40	80
N_2 purity	96.58%	96.28%	96.19%	96.16%
N_2 recovery	99.26%	99.26%	99.28%	99.29%
CO_2 purity	95%	94.95%	95.04%	95.07%
CO_2 recovery	80.09%	78.26%	77.70%	77.51%

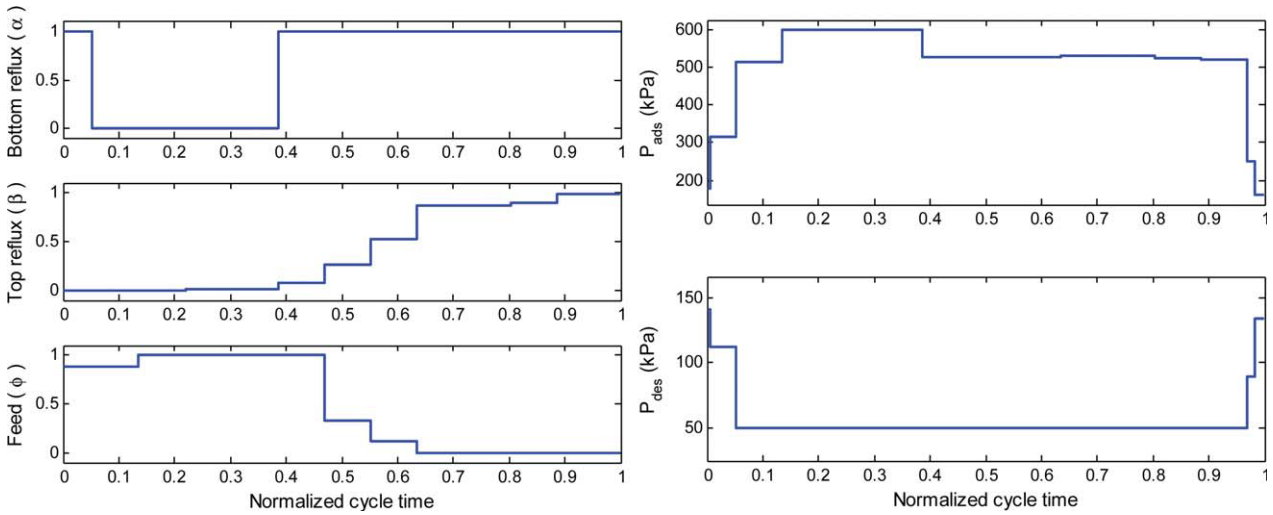

Figure 8. Optimal control profiles for Case 3.

[Color figure can be viewed in the online issue, which is available at www.interscience.wiley.com.]

CO_2 recovery for each lower bound. As a result, it is possible that a different optimal cycle configuration is achieved at each point plotted on the curve. However, each configuration is the best possible cycle for a particular CO_2 purity. Consequently, this yields an optimal purity-recovery trade-off curve. The curve shows that if a very high purity CO_2 separation is desired then the recovery falls drastically. A similar trend is observed with the purity when a very high CO_2 recovery is sought. The intermediate section of the curve is a preferable region to operate.

Case 3: Cycle synthesis to minimize power consumption

Although we achieved a high purity separation in the previous case, the power consumption was also quite high. Therefore, the objective of this case is to obtain an optimal configuration which yields a high-purity separation at minimal power requirements. To achieve this, a few small modifications are done to the NLP (18). Although the lower bound on CO_2 recovery is relaxed to 85%, the lower bounds on CO_2 purity and feed flux are relaxed to 90% and 65 kg-mol m^{-2} h^{-1}, respectively. To minimize the work done in compressing flue gas from P_{atm} to P_{feed} (in Eq. 15a), we consider P_{feed} a decision variable instead of fixing it to 300 kPa. Appropriate bounds are imposed on P_{feed}. The efficiency is kept same as 72% for all compressors and vacuum generator. The rest of the optimization problem remains same, and is as below.

$$
\begin{aligned}
&\min \\
&\quad \text{Power (from Eq. 15b)} \\
&\text{s.t.} \\
&\quad c(w) = 0 \text{ (fully discretized Eqs. 2–13)} \\
&\quad CO_2 \text{ purity} \geq 0.9 \text{ (from Eq. 14b)} \\
&\quad CO_2 \text{ recovery} \geq 0.85 \text{ (from Eq. 14d)} \\
&\quad Q_{\text{feed,L}} + Q_{\text{feed,H}} \geq 65 \text{ kg-mol m}^{-2}\text{ h}^{-1} \\
&\quad P_{\text{ads}} \geq P_{\text{d}} \\
&\quad P_{\text{des}} \leq P_{\text{feed}} \\
&\quad P_{\text{a}} \geq P_{\text{feed}} \\
&\quad 0 \leq \alpha(t_i), \beta(t_i), \phi(t_i) \leq 1 \qquad \forall t_i \\
&\quad 20 \text{ s} \leq T_{\text{c}} \leq 2400 \text{ s} \\
&\quad 101.32 \text{ kPa} \leq P_{\text{feed}} \leq 600 \text{ kPa} \\
&\quad 101.32 \text{ kPa} \leq P_{\text{ads}}(t_i) \leq 600 \text{ kPa} \qquad \forall t_i \\
&\quad P_{\text{des}}(t_i) \geq 50 \text{ kPa} \qquad \forall t_i
\end{aligned}
\tag{19}
$$

The NLP was solved in AMPL with 24 temporal finite elements and 20 spatial finite volumes. The optimal control profiles are shown in Figure 8. Although the profiles for the top and the bottom reflux are quite similar to the previous case, we observe a stark difference in the profiles of the operating pressures and the feeding strategy. As a result, we obtain an entirely different 2-bed 8-step VSA configuration, illustrated in Figure 9.

The cycle begins with $\alpha(t) = 1$, $\beta(t) = 0$ and $\phi(t)$ close to one. This suggests a heavy reflux from CnB to CoB and feed being fed to CoB. From the profiles of $P_{\text{ads}}(t)$ and $P_{\text{des}}(t)$, the pressure rises in CoB and falls in CnB during this step. Thus, we have a pressurization step for CoB (step 1) and a depressurization step for CnB (step 5). The heavy reflux increases the adsorbed-phase CO_2 concentration towards the heavy end of CoB, which is evident from the gas-phase CO_2 concentration profile for step 1 in Figure 10. Next, both $\alpha(t)$ and $\beta(t)$ go to zero, while $P_{\text{ads}}(t)$ and $P_{\text{des}}(t)$ attain their maximum and minimum allowed values,

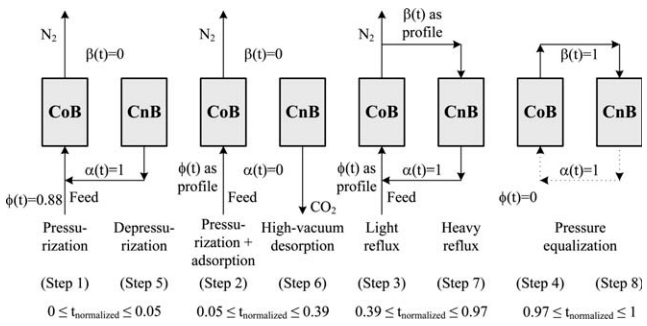

Figure 9. Optimal VSA configuration for Case 3.

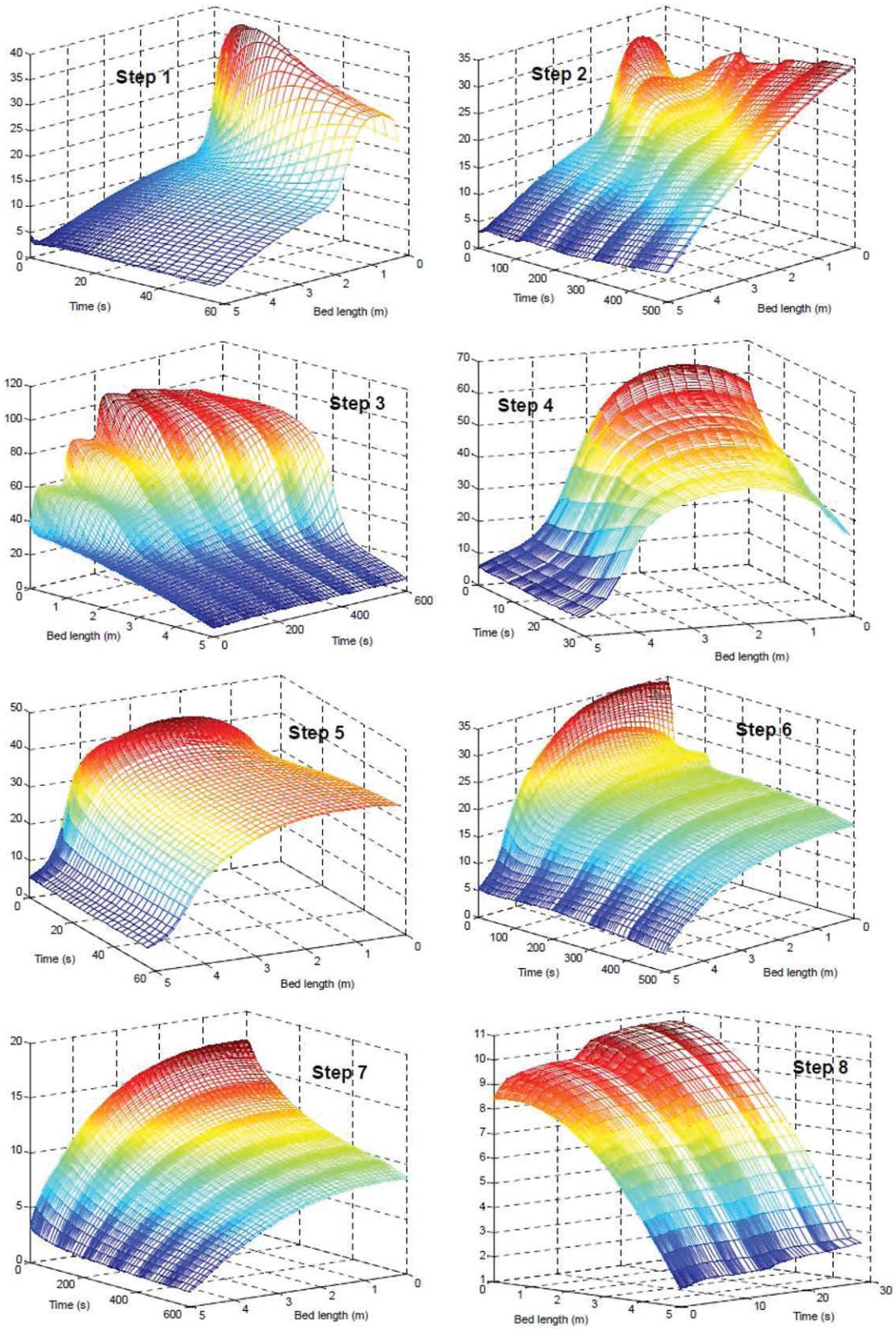

Figure 10. Gas-phase CO_2 concentration profiles for Case 3.

[Color figure can be viewed in the online issue, which is available at www.interscience.wiley.com.]

respectively. This suggests an adsorption step with the removal of light product for CoB (step 2), and a high vacuum desorption step for CnB (step 6), during which high purity CO_2 is collected. After this step, we observe that both $\alpha(t)$ and $\beta(t)$ go to 1. However, unlike the total reflux step in previous case study, $\beta(t)$ doesn't go to 1 at once and nitrogen is

Table 7. Optimization Results for Case 3

No. of variables	46313
No. of equations	46122
CPU time	273.08 min
Optimal step times	
Step 1 (and 5)	56.77 s
Step 2 (and 6)	500.03 s
Step 3 (and 7)	614.79 s
Step 4 (and 8)	28.41 s
Optimal cycle time	2400 s
Optimal P_{feed}	182.31 kPa
Feed flux	65 kg-mol m^{-2} h^{-1}
Power consumption	464.76 kWh $tonne^{-1}$ CO_2
CO_2 purity	90%
CO_2 recovery	85%

still constantly removed from the system. Feed is also fed to CoB for a considerable amount of time at the beginning of this step. Therefore, this translates into a heavy reflux step for CoB (step 3) and a light reflux step for CnB (step 7). Nevertheless, the intent of this step is similar to that of the total reflux step: enrich the N_2 front towards the light end of CnB, and CO_2 front towards the heavy end of CoB. The gas phase CO_2 concentration profiles for both these steps in Figure 10 validate this behavior.

In the previous case, the total reflux step occurred with $P_{ads}(t)$ and $P_{des}(t)$ operating at their upper and lower bounds, respectively. In contrast, CoB in this case operates at a lower $P_{ads}(t)$ instead, which leads to savings in power consumption. Another power-saving aspect of this 2-bed 8-step VSA cycle is the pressure equalization step. After the third step, $\alpha(t)$ and $\beta(t)$ remain at 1, while $P_{ads}(t)$ starts to drop, $P_{des}(t)$ starts to jump sharply, and the two pressures come very close to each other. In fact, $P_{ads}(t)$ and $P_d(t)$ are approximately equal during this step. This translates into a short pressure equalization step (step 4 and 8). Since the heavy reflux from CnB is negligible, we show it as a dotted line for this step in Figure 9. Clearly, from Figure 10, CO_2 concentration drops substantially in CoB and rises steadily in CnB during the equalization step. After this, CoB follows the steps of CnB and vice-versa.

Table 7 summarizes the optimization results. With 46,313 variables and 191 degrees of freedom in the NLP, the optimal solution was obtained in 4.5 CPU hours. At the optimum, the feed flux, CO_2 purity, and CO_2 recovery were at their respective lower bounds of 65 kg-mol m^{-2} h^{-1}, 90% and 85%. Under these conditions, and at an optimum P_{feed} of 182.3 kPa, we achieved a power consumption of 464.76 kWh $tonne^{-1}$ CO_2 captured, which is over 27% lower than Case 2. Table 8 lists a validation of the optimal results obtained from AMPL with accurate simulations in MATLAB for varying number of spatial finite volumes. As observed in the previous case, the purities and recoveries are in reasonable agreement, even for large number of finite volumes.

Figure 11 shows the trade-off curve between power consumption and CO_2 recovery. As in the previous case, we construct the curve by varying the lower bound on CO_2 recovery, while keeping purity at 90%, and optimizing NLP (19) multiple times. Thus, we obtain an optimal trade-off curve, although it is possible to obtain a different optimal cycle configuration at each point plotted on the curve. As expected, the curve shows that the power requirements increase if a high-recovery separation is desired. However, the increase is almost linear up to a recovery level of 84%. The power requirements then start growing exponentially if more than 84% CO_2 recovery is sought.

Conclusions

A fairly extensive review of the previous work on post-combustion CO_2 capture reveals that a systematic methodology is still required for the design of PSA cycles. To address this, we introduce an optimal control based framework to develop optimal PSA cycle configurations. A novel 2-bed PSA superstructure is presented which is able to predict a number of different PSA operating steps. The bed connections in the superstructure are governed by time-dependent control variables, such as the fractions of light and heavy product recycle between the beds, or the amount of feed to the beds. Different operating steps are accomplished by the superstructure by varying these control variables. To achieve an optimal sequence of operating steps, an optimal control problem, with a PDAE-based model of the PSA system and the cyclic steady state condition, is formulated.

The superstructure approach is illustrated for three case studies of post-combustion CO_2 capture. The first case study optimizes the standard 2-bed 4-step Skarstrom cycle, and shows that such conventional cycles, which focus on separating light product at a high purity, fail to produce heavy product at a high purity because of the absence of a heavy reflux step. To obtain high-purity separation, the superstructure is optimized in the second case study. A 2-bed 6-step VSA cycle is derived from the solution of the optimal control problem. With this configuration, we are able to recover about 80% of CO_2 at a substantially high purity of 95%, and at a significantly high feed flux of 80 kg-mol m^{-2} h^{-1}, but with a power consumption of 637 kWh $tonne^{-1}$ CO_2 captured. Thus, in the third case study, we focus on developing optimal configuration which yields high-purity separation with minimal power requirements. We construe a 2-bed 8-step VSA configuration from the optimal profiles, with which, at 90% purity and 85% recovery, CO_2 is extracted with a substantially low power consumption of 465 kWh $tonne^{-1}$ CO_2 captured. Hence, with the proposed superstructure approach, we are able to design optimal configurations that make pressure swing adsorption a promising option for high purity CO_2 capture from flue gas streams.

Table 8. Accuracy Validation for AMPL Results of Case 3

		MATLAB Verification		
Spatial Finite Volumes	AMPL Results 20	20	40	80
N_2 purity	97.38%	97.16%	97.03%	96.99%
N_2 recovery	98.33%	98.36%	98.40%	98.42%
CO_2 purity	90%	90.01%	90.16%	90.22%
CO_2 recovery	85%	83.72%	82.93%	82.68%

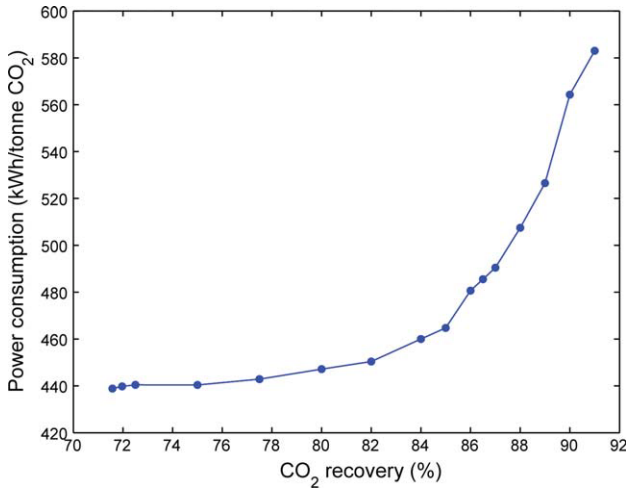

Figure 11. Power-recovery trade-off curve, at 90% CO_2 purity, for Case 3.

[Color figure can be viewed in the online issue, which is available at www.interscience.wiley.com.]

A complete discretization approach is used to solve the optimal control problem as a large-scale nonlinear program, using the nonlinear optimization solver IPOPT. Verifications of the accuracy of the discretization scheme show this approach is reasonably accurate in capturing the dynamics of PSA systems governed by hyperbolic PDAEs and steep adsorption fronts, and can be used for PSA systems with efficient NLP solvers like IPOPT. In future, a sensitivity-based sequential approach, similar to Jiang et al.[37] will also be developed to solve the optimal control problem for the superstructure without a separate verification step. Instead, the PDAEs for the PSA system will be decoupled from the optimization problem, and the partially discretized PDAEs, together with the sensitivities of the state variables with respect to decision variables, will be integrated outside the optimization problem using a sophisticated dynamic simulator which is able to capture the state variable profiles with high accuracy. The optimization problem will then be solved for the decisions using these sensitivities.

Finally, our superstructure based methodology, demonstrated for CO_2 capture in this work, is quite generic and can be extended to many other PSA applications; no assumptions are made on the adsorbent or feedstock, the operating steps that can be predicted, or details of the bed models. This makes the approach fairly general. Moreover, the superstructure can also be used to evaluate different kinds of adsorbents for the same feedstock and process conditions. Although the current superstructure involves only two beds, we also plan to extend the formulation to a superstructure incorporating more beds, more complex flow patterns and more challenging multi-component mixtures.

Acknowledgments

This technical effort was performed in support of the National Energy Technology Laboratory's on-going research in Process and Dynamic Systems Research under the RDS contract DE-AC26-04NT41817.

Notation

BR_i = flux of ith component in the bottom reflux stream (g-mol m^{-2} s^{-1})
C_i = gas-phase concentration of ith component (g-mol m^{-3})
C^i_{pg} = heat capacity of ith component (J g-mol^{-1} K^{-1})
C_{ps} = heat capacity of the adsorbent (J kg^{-1} K^{-1})
d_p = particle diameter (m)
F_i = input flux of ith component to the co-current bed (g-mol m^{-2} s^{-1})
h = total gas-phase enthalpy (J m^{-3})
ΔH^{ads}_i = isosteric heat of adsorption (J g-mol^{-1})
HP_i = flux of ith component in the heavy product stream (g-mol m^{-2} s^{-1})
k_i = lumped mass transfer coefficient for ith component (s^{-1})
LP_i = flux of ith component in the light product stream (g-mol m^{-2} s^{-1})
M^i_w = molecular weight of ith component (kg g-mol^{-1})
P = total bed pressure (kPa)
P_{ads} = pressure at the light end of the co-current bed (kPa)
P_{des} = pressure at the heavy end of the counter-current bed (kPa)
q_i = solid-phase concentration of ith component (g-mol kg^{-1})
q^*_i = equilibrium solid-phase concentration of ith component (g-mol^{-1} kg^{-1})
T = gas-phase temperature in the bed (K)
T_w = wall/ambient temperature (K)
TR_i = flux of ith component in the top reflux stream (g-mol m^{-2} s^{-1})
U_A = effective heat transfer coefficient (J m^{-3} s^{-1} K^{-1})
v = gas superficial velocity (m s^{-1})
W_{total} = total work done by the compressors and the vacuum generator (J m^{-2} s^{-1})

Greek letters

α = fraction of the heavy product going as a bottom reflux
β = fraction of the light product going as a top reflux
γ = heat capacity ratio (=1.4)
ε_b = bulk void fraction
ϕ = fraction of the feed going to the co-current bed
μ = gas viscosity (kg m^{-1} s^{-1})
η_c = efficiency of the feed compressor
η_{fg} = efficiency of the flue gas compressor
η_h = efficiency of the heavy product compressor
η_v = efficiency of the vacuum generator
ρ_b = bulk density (kg m^{-3})
ρ_s = adsorbent density (kg m^{-3})

Literature Cited

1. IEA/WEO. *World Energy Outlook 2006 tech. rep.*, Paris, France: International Energy Agency; 2006.
2. Aaron D, Tsouris C. Separation of CO_2 from flue gas: a review. *Separ Sci Technol*. 2005;40:321–348.
3. IPCC.*Carbon Dioxide Capture and Storage tech. rep*. Geneva, Switzerland: Intergovernmental Panel on Climate Change; 2005.
4. Sircar S, Kratz WC. Simultaneous production of hydrogen and carbon dioxide from steam reformer off-gas by pressure swing adsorption. *Separ Sci and Technol*. 1988;23:2397–2415.
5. Kumar R. Removal of water and carbon dioxide from atmospheric air. US Patent 4,711,645, 1987.
6. Tamura T. Absorption process for gas separation. US Patent 3,797,201, 1974.
7. Hirose M, Omori I, Oba M, Kawai T. Carbon dioxide separation and recovery system. Jpn Patent 2005262001, 2005.
8. Ishibashi M, Ota H, Akutsu N, Umeda S, Tajika M, Izumi J, Yasutake A, Kabata T, Kageyama Y. Technology for removing carbon dioxide from power plant flue gas by the physical adsorption method. *Energ Convers Manage*. 1996;37:929–933.
9. Ito K, Otake K, Itoi M. Carbon dioxide desorption method. Jpn Patent 2004202393, 2004.

10. Sasaki A, Matsumoto S, Fujitsuka M, Shinoki T, Tanaka T, Ohtsuki J. CO_2 recovery in molten carbonate fuel cell system by pressure swing adsorption. *IEEE Trans Energ Convers.* 1993;8:26–32.
11. Yokoyama T. Japanese R&D on Large-Scale CO_2 Capture in *ECI Symposium Series on Separations Technology VI: New Perspectives on Very Large-Scale Operations*; RP3 2004.
12. Reynolds SP, Ebner AD, Ritter JA. Stripping PSA cycles for CO_2 recovery from flue gas at high temperature using a hydrotalcite-like adsorbent. *Ind Eng Chem Res.* 2006;45:4278–4294.
13. Reynolds S, Mehrotra A, Ebner A, Ritter J. Heavy reflux PSA cycles for CO2 recovery from flue gas: Part I. Performance Evaluation. *Adsorption.* 2008;14:399–413.
14. Kikkinides ES, Yang RT, Cho SH. Concentration and recovery of carbon dioxide from flue gas by pressure swing adsorption. *Ind Eng Chem Res.* 1993;32:2714–2720.
15. Chue KT, Kim JN, Yoo YJ, Cho SH, Yang RT. Comparison of activated carbon and zeolite 13X for CO_2 recovery from flue gas by pressure swing adsorption. *Ind Eng Chem Res.* 1995;34:591–598.
16. Takamura Y, Narita S, Aoki J, Hironaka S, Uchida S. Evaluation of dual-bed pressure swing adsorption for CO_2 recovery from boiler exhaust Gas. *Separ Purif Technol.* 2001;24:519–528.
17. Park JH, Beum HT, Kim JN, Cho SH. Numerical analysis on the power consumption of the PSA process for recovering CO_2 from flue gas. *Ind Eng Chem Res.* 2002;41:4122–4131.
18. Gomes VG, Yee KWK. Pressure swing adsorption for carbon dioxide sequestration from exhaust gases. *Sep Purifi Technol.* 2002; 28:161–171.
19. Na BK, Koo KK, Eum HM, Lee H, Song H. CO_2 recovery from flue gas by PSA process using activated carbon. *korean J Chem Eng.* 2001;18:220–227.
20. Na BK, Lee H, Koo KK, Song HK. Effect of rinse and recycle methods on the pressure swing adsorption process to recover CO_2 from power plant flue gas using activated carbon. *Ind Eng Chem Res.* 2002;41:5498–5503.
21. Choi WK, Kwon TI, Yeo YK, Lee H, Song H, Na BK. Optimal operation of the pressure swing adsorption (PSA) process for CO_2 recovery. *Korean J Chem Eng.* 2003;20:617–623.
22. Chou CT, Chen CY. Carbon dioxide recovery by vacuum swing adsorption. *Separ Purif Technol.* 2004;39:51–65.
23. Ko D, Siriwardane R, Biegler LT. Optimization of pressure swing adsorption and fractionated vacuum pressure swing adsorption processes for CO_2 capture. *Ind Eng Chem Res.* 2005;44:8084–8094.
24. Grande CA, Cavenati S, Rodrigues AE. Pressure swing adsorption for carbon dioxide sequestration presented at ENPROMER 2005, 4th Mercosur Conference on Process Systems Engineering, Rio de Janeiro, Brasil, 2005.
25. Chaffee AL, Knowles GP, Liang Z, Zhang J, Xiao P, Webley PA. CO_2 capture by adsorption: materials and process development. *Int J Greenhouse Gas Control.* 2007;1:11–18.
26. Zhang J, Webley PA, Xiao P. Effect of process parameters on power requirements of vacuum swing adsorption technology for CO_2 capture from flue gas. *Energ Conver Manage.* 2008;49:346–356.
27. Xiao P, Zhang J, Webley PA, Li G, Singh R, Todd R. Capture of CO_2 from flue gas streams with zeolite 13X by avacuum-pressure swing adsorption. *Adsorption.* 2008;14:575–582.
28. Reynolds SP, Ebner AD, Ritter JA. New pressure swing adsorption cycles for carbon dioxide sequestration. *Adsorption.* 2005; 11:531–536.
29. Reynolds SP, Ebner AD, Ritter JA. Carbon dioxide capture from flue gas by pressure swing adsorption at high temperature using a K-promoted HTlc: effects of mass transfer on the process performance. *Environ Prog.* 2006;25:334–342.
30. Zhang J, Webley PA. Cycle development and design for CO_2 capture from Flue gas by vacuum swing adsorption. *Environ Sci Technol.* 2008;42:563–569.
31. Chiang AST. Arithmetic of PSA process scheduling. *AIChE J.* 1988;34:1910–1912.
32. Smith OJ, Westerberg AW. Mixed-integer programming for pressure swing adsorption cycle scheduling. *Chemi Eng Sci.* 1990;45: 2833–2842.
33. Smith OJ, Westerberg AW. The optimal design of pressure swing adsorption systems. *Chem Eng Sci.* 1991;46:2967–2976.
34. Smith OJ, Westerberg AW. The optimal design of pressure swing adsorption systems–II. *Chem Eng Sci.* 1992;47:4213–4217.
35. Kumar R, Fox VG, Hartzog D, et al. A versatile process simulator for adsorptive separations. *Chem Eng Sci.* 1994;49:3115–3125.
36. Skarstrom CW. Method and apparatus for fractionating gaseous mixtures by adsorption US Patent 2,944,627, 1960.
37. Jiang L, Fox VG, Biegler LT. Simulation and optimal design of multiple-bed pressure swing adsorption systems. *AIChE.* 2004; 50:2904–2917.
38. Ruthven DM, Farooq S, Knaebel KS. *Pressure Swing Adsorption.* VCH Publishers, Inc, New York, 1994.
39. Sircar S, Hufton JR. Why does the linear driving force model for adsorption kinetics work? *Adsorption.* 2000;6:137–147.
40. Balakrishna S, Biegler LT. Targeting strategies for the synthesis and energy integration of nonisothermal reactor networks. *Ind Eng Chem Res.* 1992;31:2152–2164.
41. Biegler LT, Cervantes AM, Wächter A. Advances in simultaneous strategies for dynamic process optimization. *chem Eng Sci.* 2002;57:575–593.
42. Wächter A, Biegler LT. On the implementation of an Interior-point filter line-search algorithm for large-scale nonlinear programming. *Math Program.* 2006;106:25–57.
43. LeVeque RJ. *Numerical Methods for Conservation Laws*. Birkhäuser, Basel, 1992.
44. Webley PA, He J. Fast solution-adaptive finite volume method for PSA/VSA cycle simulation; 1 Single step simulation. *Comput Chem Eng.* 2000;23:1701–1712.
45. Kameswaran S, Biegler LT. Convergence rates for direct transcription of optimal control problems using collocation at radau points. *Comput Optimi Appli.* 2008;41:81–126.
46. *MATLAB User's Guide*. The Mathworks, Inc., Natick, MA, 1994–2005.
47. Kameswaran S, Biegler LT. Simultaneous dynamic optimization strategies: recent advances and challenges. *Comput Chem Eng.* 2006;30:1560–1575.
48. Fourer R, Gay DM, Kernighan BW. A modeling language for mathematical programming. *Manage Sci.* 1990;36:519–554.

Manuscript received Mar. 25, 2009, revision received July 31, 2009, and final revision received Oct. 1, 2009.